Inorganic Chemistry

Article

pubs.acs.org/IC

# Systematic Study of a Family of Butterfly-Like $\{M_2Ln_2\}$ Molecular Magnets (M = $Mg^{II}$, $Mn^{III}$, $Co^{II}$, $Ni^{II}$, and $Cu^{II}$; Ln = $Y^{III}$, $Gd^{III}$, $Tb^{III}$, $Dy^{III}$, $Ho^{III}$, and $Er^{III}$)

Eufemio Moreno Pineda,[†] Nicholas F. Chilton, Floriana Tuna, Richard E. P. Winpenny,* and Eric J. L. McInnes*

School of Chemistry and Photon Science Institute, The University of Manchester, Oxford Road, Manchester M13 9PL, United Kingdom

Supporting Information

**ABSTRACT:** A family of 3d−4f $[M^{II}_2Ln^{III}_2(\mu_3\text{-}OH)_2(O_2C^tBu)_{10}]^{2-}$ "butterflies" (where $M^{II}$ = Mg, Co, Ni, and Cu; $Ln^{III}$ = Y, Gd, Tb, Dy, Ho, and Er) and $[Mn^{III}_2Ln^{III}_2(\mu_3\text{-}O)_2(O_2C^tBu)_{10}]^{2-}$ molecules (where $Ln^{III}$ = Y, Gd, Tb, Dy, Ho, and Er) has been synthesized and characterized through single-crystal X-ray diffraction, SQUID magnetometry, and ab initio calculations. All dysprosium- and some erbium-containing tetramers showed frequency-dependent maxima in the out-of-phase component of the susceptibility associated with slow relaxation of magnetization, and hence, they are single-molecule magnets (SMMs). AC susceptibility measurements have shown that the SMM behavior is entirely intrinsic to the Dy and Er sites and the magnitude of the energy barrier is influenced by the interactions between the 4f and the 3d metal. A trend is observed between the strength of the 3d-4f exchange interaction between and the maximum observed in the $\chi''_M(T)$.

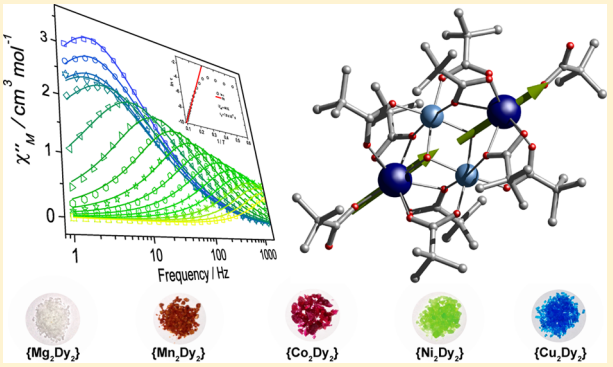


## INTRODUCTION

Much research involving the synthesis of molecular nanoclusters has taken place since it was demonstrated that such systems could retain magnetization purely at the molecular level.[1] Molecules possessing these characteristics display hysteresis and are considered potential candidates for use in data storage, spintronics, and quantum computing devices.[2] Initially most of the effort concentrated on 3D-metal clusters displaying a large spin ground state ($S$) and high negative zero-field splitting ($D$), with studies of manganese clusters most common.[3]

Investigation of the magnetism of lanthanide complexes arose from the discovery that monometallic complexes of 4f ions can also show slow relaxation of magnetization; the most studied compounds are the double-decker phthalocyaninato−lanthanide complexes.[4] These molecules opened up a new era for single-molecule magnets (SMMs),[5] where the observed behavior was due to the large magnetic moments and inherent anisotropy of lanthanide ions.[6] Lanthanides have shown higher energy barriers than observed for transition metal ions, for example, $[Tb^{III}(Pc)_2]$ is an SMM consisting of a single ion with a barrier of 938 K,[7] while a value of 842 K was obtained for Dy(III) doped in $[Y^{III}_4K_2O(O^tBu)_{12}]$.[8]

The magnetic behavior of lanthanide clusters is complex, and the importance of magnetic change in such clusters is poorly understood at present. At a single-ion level the *Ising* anisotropy is mainly dependent on the ligand field and geometry, whereas in polymetallic systems the ligand field, exchange interactions, geometry, and relative orientation of single sites in the cluster are some of the factors that determine the magnetic behavior.[6] Despite having large magnetic moments and anisotropy and showing slow relaxation of magnetization, lanthanide complexes do not generally show wide hysteresis loops due to their fast quantum tunnelling of the magnetization (QTM) at zero external field. This can be suppressed when other interactions are introduced. For example, suppression of the quantum tunnelling process in Ln-based SMMs at zero field has been addressed by introducing radicals as bridging ligands. Rinehart et al. employed this approach in Dy(III) and Tb(III) dimers, obtaining hysteresis up to 14 K, the highest observed for a molecule-based system.[9] Ruben and co-workers also reported hysteresis, observed by XMCD measurements, on terbium phthalocyanine complexes deposited on ferromagnetic nickel supports up to 100 K.[10]

The study of the magnetic behavior of 3d metals combined with lanthanides was pioneered by the Gatteschi group in the 1980s[11a−c] and in the 1990s by ourselves[11d] and others.[11] Recently, it has re-emerged as a method to combine the large anisotropic character imposed for lanthanides, i.e., Tb(III), Dy(III), Ho(III), and Er(III), while strong magnetic interactions can be promoted by 3d ions, therefore improving the dynamic

**Received:** April 5, 2015
**Published:** May 27, 2015

ACS Publications © 2015 American Chemical Society



DOI: 10.1021/acs.inorgchem.5b00746
*Inorg. Chem.* 2015, 54, 5930−5941

properties of SMMs.[12] Many interesting 3d−4f molecules have been reported; however, little is known about the exchange interaction ($J_{3d-4f}$) between the mixed-metal pair when the lanthanide center is a highly anisotropic system, limiting most of the research to the isotropic Gd(III) analogues[11] and just a few examples of studies of interaction between highly anisotropic lanthanides and 3d metals.[13] Insight into the exchange interactions between 3d metals with anisotropic lanthanides has become achievable through the use of multiconfigurational ab initio calculations of the complete active space self consistent field (CASSCF) variety.[8,12,13] Furthermore, experimentally astonishing work by means of high-field electron paramagnetic resonance (HF-EPR) combined with pulsed-field magnetization studies has shed some light into the direct determination of the exchange interaction between 3d−4f systems, with Ln(III) = Tb, Dy, Ho, and/or Er.[14]

Many factors play a key role in the relaxation mechanism(s) in lanthanide-based systems, ranging from ligand set and lanthanide geometry to exchange interactions; therefore, a better understanding of the parameters that affect the magnetic behavior of such systems is a key requirement toward development of better SMMs and their potential exploitation. With this in mind, herein we report the synthesis and magnetic properties of a family of heterotetrametallic $\{M_2Ln_2\}$ cage compounds, each comprising two 3d (M) and two 4f (Ln) centers, where M = Mn(III), Co(II), Ni(II), and Cu(II) and Ln = Gd(III), Tb(III), Dy(III), Ho(III), and Er(III). In addition we also report the $\{Mg_2Ln_2\}$ and $\{M_2Y_2\}$ analogues, where Mg(II) and Y(III) are diamagnetic.

3d−4f butterflies have been investigated since the late 1990s[15] with the first 3d−4f SMMs reported by Brechin and Christou.[16] Since that time beautiful systematic studies have been performed, chiefly by the Murray group, examining largely $Co^{III}_2$−$Ln_2$ and $Cr^{III}_2$−$Ln_2$ butterflies,[17] and the Powell group, which has focused on $Fe^{III}_2$−$Ln_2$ butterflies.[18] There have been some further interesting excursions into $Co^{II}_2Ln_2$, $Ni^{II}_2Ln_2$, and $Mn^{III}_2Ln_2$ cages.[19] Here we attempted to be more inclusive, studying the magnetic behavior of a near-complete grid of 27 complexes (with only the $\{Cu_2Tb_2\}$ and $\{Cu_2Y_2\}$ members missing; $\{Mg_2Y_2\}$ is neglected as it is entirely diamagnetic). Thus, we can systematically probe the interaction between the 3d and the 4f ions and the effects on SMM behavior. We conclude that any magnetic interaction between M and Ln diminishes the energy barrier for magnetic relaxation in these molecules.

## EXPERIMENTAL SECTION

**Synthesis.** Unless stated otherwise, all reagents and solvents were purchased and used without further purification. Syntheses of inorganic starting materials, $[M^{II}_2(\mu\text{-}OH_2)(O_2C^tBu)_4(HO_2C^tBu)_4]$ ($M^{II}$ = Mg, Co, and Ni),[20a−c] $[Mn^{II}_2(O_2C^tBu)_4EtOH]_n$,[20d] $[Cu^{II}_2(O_2C^tBu)_4(HO_2C^tBu)_2]$,[20e] and $[Ln^{III}_2(O_2C^tBu)_6(HO_2C^tBu)_6]$[20f,g] ($Ln^{III}$ = Y, Gd, Tb, Dy, Ho, and Er), were carried out by literature methods (see Table S1, Supporting Information).

A total of 27 mixed-metal tetramers was synthesized through two different methods, described below.

**Method A.** *$[Mg^{II}_2Ln^{III}_2(\mu_3\text{-}OH)_2(O_2C^tBu)_{10}][^iPr_2NH_2]_2$.* $[Mg^{II}_2(\mu\text{-}OH_2)(O_2C^tBu)_4(HO_2C^tBu)_4]$ (0.1 g, 0.1 mmol), $[Ln^{III}_2(O_2C^tBu)_6(HO_2C^tBu)_6]$ ($Ln^{III}$ = Gd (**1**), Tb (**2**), Dy (**3**), Ho (**4**), and Er (**5**)) (0.1 mmol), and diisopropylamine ($^iPr_2NH$) (0.1 mL, 0.7 mmol) in acetonitrile (MeCN) (8 mL) were stirred at room temperature for 5 min. The resulting solution was transferred into a 10 mL Teflon-lined autoclave, which was heated at 150 °C for 12 h and then cooled to room temperature at a rate of 0.05 °C $min^{-1}$. Colorless X-ray quality crystals were obtained directly from the autoclave.

*$[Co^{II}_2Ln^{III}_2(\mu_3\text{-}OH)_2(O_2C^tBu)_{10}][^iPr_2NH_2]_2$.* $[Co^{II}_2(\mu\text{-}OH_2)(O_2C^tBu)_4(HO_2C^tBu)_4]$ (0.1 g, 0.1 mmol), $[Ln^{III}_2(O_2C^tBu)_6(HO_2C^tBu)_6]$ ($Ln^{III}$ = Y (**6**), Gd (**7**), Tb (**8**), Dy (**9**), Ho (**10**), and Er (**11**)) (0.1 mmol), and $^iPr_2NH$ (0.1 mL, 0.7 mmol) in MeCN (8 mL) were stirred at room temperature for 5 min. The resulting solution was transferred into a 10 mL Teflon-lined autoclave, which was heated at 150 °C for 12 h and then cooled to room temperature at a rate of 0.05 °C $min^{-1}$. The resulting solution was then filtered and left undisturbed. Pink X-ray quality crystals were obtained after 48 h.

*$[Mn^{III}_2Ln^{III}_2(\mu_3\text{-}O)_2(O_2C^tBu)_{10}][Et_3NH]_2$.* $[Mn^{II}_2(O_2C^tBu)_4EtOH]_n$ (0.1 g, 0.5 mmol), $[Ln^{III}_2(O_2C^tBu)_6(HO_2C^tBu)_6]$ ($Ln^{III}$ = Y (**12**), Gd (**13**), Tb (**14**), Dy (**15**), Ho (**16**), and Er (**17**)) (0.1 mmol), and triethylamine ($Et_3N$) (0.1 mL, 0.5 mmol) in MeCN (8 mL) were stirred at room temperature for 5 min. The resulting solution was transferred into a 10 mL Teflon-lined autoclave, which was heated at 150 °C for 12 h and then cooled to room temperature at a rate of 0.05 °C $min^{-1}$. The resulting solution was then filtered and left undisturbed. Orange X-ray quality crystals were obtained after 72 h.

**Method B.** *$[Ni^{II}_2Ln^{III}_2(\mu_3\text{-}OH)_2(O_2C^tBu)_{10}[Et_3NH]_2$.* To a stirred solution of $[Ni^{II}_2(\mu\text{-}OH_2)(O_2C^tBu)_4(HO_2C^tBu)_4]$ (0.2 g, 0.2 mmol) and $[Ln^{III}_2(O_2C^tBu)_6(HO_2C^tBu)_6]$ ($Ln^{III}$ = Y (**18**), Gd (**19**), Tb (**20**), Dy (**21**), Ho (**22**), and Er (**23**)) (0.2 mmol) in MeCN (20 mL) was added $Et_3N$ (0.2 mL, 1.4 mmol) after 15 min. The resulting solution was heated to reflux for a period of 3 h. The solution was then cooled to room temperature and filtered. Yellow-green X-ray quality crystals were obtained directly from slow evaporation after 24 h.

*$[Cu^{II}_2Ln^{III}_2(\mu_3\text{-}OH)_2(O_2C^tBu)_{10}][^iPr_2NH_2]_2$.* To a stirred solution of $[Cu^{II}_2(O_2C^tBu)_4(HO_2C^tBu)_2]$ (0.15 g, 0.2 mmol) and $[Ln^{III}_2(O_2C^tBu)_6(HO_2C^tBu)_6]$ ($Ln^{III}$ = Gd (**24**), Dy (**25**), Ho (**26**), and Er (**27**)) (0.2 mmol) in MeCN (20 mL) was added $^iPr_2NH$ (0.2 mL, 1.4 mmol) after 15 min. The resulting solution was heated to reflux for a period of 3 h. The solution was cooled to room temperature and then filtered. Blue X-ray quality crystals were obtained directly from slow evaporation after 48 h.

**X-ray Data Collection and Structure Solution.** Single-crystal X-ray diffraction measurements for **7**, **9**, **15**, **19**, **21**, **24**, and **25** were carried out on an Oxford Xcalibur CCD diffractometer with Mo K$\alpha$ radiation ($\lambda$ = 0.71073 Å). Data collection of **1**, **3**, **5**, **12**, **13**, **18**, and **23** was carried out on an Agilent SUPERNOVA diffractometer with Mo K$\alpha$ radiation ($\lambda$ = 0.71073 Å). Data reduction and unit cell refinement were performed with CrysAlisPro software. The structures were solved by direct methods using SHELXS-97[21a] and refined by full-matrix least-squares methods using Olex2.[21b] In all cases the crystals were mounted on a tip using crystallographic oil and placed in a cryostream. Data were collected using $\phi$ and $\omega$ scans chosen to give a complete asymmetric unit. All non-hydrogen atoms were refined anisotropically, while hydrogen atoms were calculated geometrically and refined in riding mode. Crystal data and refinement parameters are given in Tables S2−S4, Supporting Information. CCDC 1050247−1050260 contains the supplementary crystallographic data for this paper. These data can be obtained free of charge via www.ccdc.cam.ac.uk/conts/retrieving.html (or from Cambridge Crystallographic Data Centre, 12 Union Road, Cambridge CB21EZ, U.K.; fax (+44)1223-336-033; deposit@ccdc.cam.ac.uk).

**Magnetic Measurements.** The magnetic properties of polycrystalline samples of **1**−**27** were measured with a Quantum Design MPMS-XL7 SQUID magnetometer. The samples were ground, placed in a gel capsule, and fixed with a small amount of eicosane to avoid movement during the measurement. The data were corrected for the diamagnetism of the gel capsule and the eicosane with the diamagnetic contribution from the complexes calculated from Pascal constants.[22] Alternating current (ac) measurements were performed using a small oscillating magnetic field, 1.55 G, with and without a direct current (dc) applied magnetic field. Fitting of magnetic data used the program *PHI*.[23]

## RESULTS AND DISCUSSION

**Synthetic Dscription.** Reaction of the 3d and 4f carboxylate precursors in the presence of a mild base in acetonitrile gives a family of isostructural tetrametallic $\{M_2Ln_2\}$ clusters. The molecules feature a butterfly-like core, with an $M_2$ body and Ln wing-tips, and consist of an anion $[M^{II}_2Ln^{III}_2(\mu_3\text{-}OH)_2(O_2C^tBu)_{10}]^{2-}$ ($M^{II}$ = Mg, Co, Ni, and Cu) balanced by two diisopropylammonium ($^iPr_2NH_2^+$) or triethylammonium



DOI: 10.1021/acs.inorgchem.5b00746
Inorg. Chem. 2015, 54, 5930−5941

($Et_3NH^+$) cations. We were also able to synthesize the manganese(III) analogue with an isostructural metal core $[Mn^{III}_2Ln^{III}_2(\mu_3\text{-}O)_2(O_2C^tBu)_{10}][Et_3NH]_2$ where the two $\mu_3$-OH are substituted by two $\mu_3$-O (see later for explanation).

The $\{M_2Ln_2\}$ family was obtained from two different methods. The yield in both cases ranges between 30% and 92%. The $\{Ni_2Ln_2\}$ and $\{Cu_2Ln_2\}$ clusters were obtained by refluxing $[Ni^{II}_2(\mu\text{-}OH_2)(O_2C^tBu)_4(HO_2C^tBu)_4]$ or $[Cu^{II}_2(O_2C^tBu)_4(HOC^tBu)_2]$, respectively, with $[Ln^{III}_2(O_2C^tBu)_6(HOC^tBu)_6]$ in the presence of triethylamine or diisopropylamine, respectively. The $\{Mg_2Ln_2\}$, $\{Mn_2Ln_2\}$, and $\{Co_2Ln_2\}$ clusters were prepared under solvothermal conditions using $[Mg^{II}_2(\mu\text{-}OH_2)(O_2C^tBu)_4(HO_2C^tBu)_4]$, $[Mn^{II}_2(O_2C^tBu)_4EtOH]_n$, or $[Co^{II}_2(\mu\text{-}OH_2)(O_2C^tBu)_4(HO_2C^tBu)_4]$ and the lanthanide source in the presence of triethylamine or diisopropylamine (see Supporting Information for more details). Attempts to synthesize $\{Cu_2Y_2\}$ and $\{Cu_2Tb_2\}$ were made, but we were not able to crystallize these materials.

These represent the largest heterometallic 3d−4f family; other heterometallic 3d−4f complexes have been reported.[15b,24]

**Crystal Structures.** The complexes crystallize in three different space groups, *P*-1, *C*2/*c*, and $P2_1/c$, depending on the lanthanide metal source. The molecular structures of the complex anions are very similar in all cases and always centrosymmetric. The description of **3** is given as representative (Figure 1).

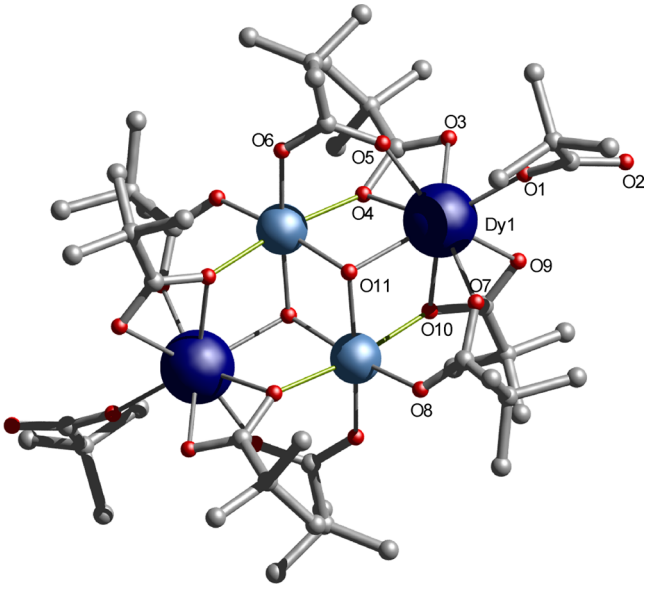


**Figure 1.** Crystal structure of $[Mg_2^{II}Dy_2^{III}(\mu_3\text{-}OH)_2(O_2C^tBu)_{10}]^{2-}$. Color scheme: Dy, blue; Mg, cyan; O, red; C, gray. H omitted for clarity.

The anionic cluster is composed of 2 Mg(II), 2 Dy(III), 2 $\mu_3$-OH ($\mu_3$-O for the Mn(III) analogue), and 10 pivalates. The cluster is charged-balanced by two $[^iPr_2NH_2^+]$ cations. In **3** the Mg(II) ion has adopted a slightly distorted octahedral geometry with an $O_6$ donor set. The Dy(III) ion was systematically analyzed using SHAPE 2.1[25] software, resulting in a distorted square antiprism geometry ($D_{4h}$, with a value of 2.323) with an $O_8$ donor set (see Table S5, Supporting Information, for geometrical parameters for other $\{M_2Dy_2\}$ analogues). The Mg(II) ion is chelated by four pivalates and two (cis) $\mu_3$-OH, while the Dy(III) ion is bridged by four pivalates, one $\mu_3$-OH, and a terminal pivalate. Hydrogen bonding is observed between the diisopropylammonium cations and the unbound oxygen of the terminal pivalates.

Complexes containing copper or manganese show a Jahn−Teller distortion along the O4−M−O10′ axis with an elongated octahedral environment typical for $d^4$ and $d^9$ metals (bond length ranges: Cu−$O_{eq}$ = 1.945(3)−1.978(2) Å, Cu−$O_{ax}$ = 2.397(2)−2.421(1) Å; bond angle ranges cis at Cu = 81.45(8)−96.09(8)°, trans at Cu = 172.46(9)−174.98(8)°. Mn−$O_{eq}$ range = 1.866(2)−1.970(2) Å, Mn−$O_{ax}$ = 2.289(2)−2.349(2) Å; bond angle ranges cis at Mn = 82.88(8)−98.38(8)°, trans at Mn = 174.10(9)−177.29(8)°) (Table 1 and Figure S1, Supporting Information).

The equatorial sites of the 3d metal are occupied by two bridging hydroxides or oxides and oxygen atoms from bridging pivalates, while oxygen atoms from the Dy-chelating pivalates fill the axial sites. The oxidation state of all manganese-containing systems was determined by consideration of its coordination geometry, bond lengths, coordination numbers, the presence of Jahn−Teller elongation axes for the manganese sites, and the magnetic properties (see later). Selected bond lengths and angles for Dy-containing complexes are listed in Table 1.

A considerably shorter M···$O_{eq}$ bond length was observed for all manganese-containing clusters compared to the other 3d analogues, e.g., Table 1. A search of the crystallographic database shows the characteristic metal−oxygen bond lengths for $\mu_3$-$OH^-$ and $\mu_3$-$O^{2-}$ groups are 1.921−2.120 and 1.838−1.918 Å, respectively. This, in addition to the presence of two triethylammonium cations, confirms that there are bridging oxides in the manganese analogues.

## MAGNETISM

**Direct Current Magnetic Susceptibility Studies.** The magnetic properties of all clusters were probed on polycrystalline samples via variable-temperature (2−300 K) susceptibility (applied dc magnetic field, $H$ = 1 kG), and variable-field (0−7 T) and -temperature (2−4 K) magnetization measurements (see below and Table S6, Supporting Information).

In order to understand how the paramagnetic 3D-metal affects the magnetic behavior of the lanthanide in the $\{M_2Ln_2\}$ clusters we first describe the $\{Mg_2Ln_2\}$ and $\{M_2Y_2\}$ examples, allowing us to independently assess the 3d···3d interactions, the 4f ion electronic structure, and possible 4f···4f interactions. We then discuss the $\{M_2Ln_2\}$ clusters where M and Ln are both paramagnetic. When Ln is the spin-only Gd(III) ($^8S_{7/2}$) ion, we can directly model and determine the 3d···4f interaction. Such exact modeling is not possible where Ln is an orbitally degenerate ion.

**Table 1. 3d Metal−Oxygen Distances Dysprosium-Containing Molecules**

| | $\{Mg_2Dy_2\}$ | $\{Mn_2Dy_2\}$ | $\{Co_2Dy_2\}$ | $\{Ni_2Dy_2\}$ | $\{Cu_2Dy_2\}$ |
|---|---|---|---|---|---|
| M···$O11_{eq}$ | 2.084(3) | 1.866(2) | 2.078(2) | 2.058(1) | 1.978(2) |
| M···$O4_{ax}$ | 2.099(3) | 2.289(2) | 2.178(2) | 2.102(2) | 2.397(2) |
| M···$O10_{ax}$ | 2.070(3) | 2.349(2) | 2.171(2) | 2.092(2) | 2.421(2) |
| M···$O6_{eq}$ | 2.036(2) | 1.975(3) | 2.041(3) | 2.029(1) | 1.945(3) |
| M···$O8_{eq}$ | 2.038(3) | 1.970(2) | 2.038(2) | 2.023(1) | 1.954(3) |



DOI: 10.1021/acs.inorgchem.5b00746
*Inorg. Chem.* 2015, 54, 5930−5941

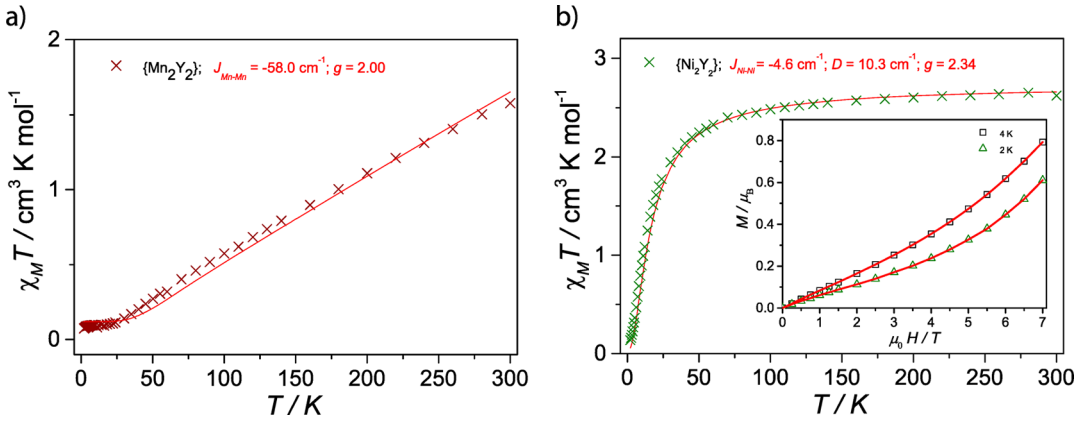


**Figure 2.** (a) Experimental $\chi_M T(T)$ data and fits for $\{Mn_2Y_2\}$; (b) experimental $\chi_M T(T)$ and $M_\beta$ $(H,T)$ (inset) data and fits for $\{Ni_2Y_2\}$.

However, we can indirectly assess the 3d···4f interactions in these examples through comparison of the $\chi_M T(T)$ behavior of $\{M_2Ln_2\}$ with the sum of those for the appropriate $\{M_2Y_2\}$ and $\{Mg_2Ln_2\}$ systems: these would be identical in the case of nil interaction, with any divergences depending on the sign and strength of interaction.

*{$M_2Y_2$}*. The magnetic behavior for $[Co^{II}{}_2Y^{III}{}_2(\mu_3\text{-}OH)_2(O_2C^tBu)_{10}](iPr_2NH)_2$, $[Ni^{II}{}_2Y^{III}{}_2(\mu_3\text{-}OH)_2(O_2C^tBu)_{10}](Et_3N)_2$, and $[Mn^{III}{}_2Y^{III}{}_2(\mu_3\text{-}OH)_2(O_2C^tBu)_{10}][Et_3N]_2$ is depicted in Figures 2 and S2, Supporting Information. For $\{Mn_2Y_2\}$ (**12**), $\chi_M T(T)$ steadily decreases from 1.76 $cm^3$ K $mol^{-1}$ at 300 K (lower than the spin-only value of 6.0 $cm^3$ K $mol^{-1}$ for two noninteracting $S = 2$ ions with $g = 2.0$) toward zero on cooling (Figure 2a). This is characteristic of an antiferromagnetic interaction, consistent with the lack of a low-temperature $M_\beta(H)$ signal, suggesting an $S = 0$ ground state. We modeled the $\chi_M T(T)$ behavior of $\{Mn_2Y_2\}$ using a simple isotropic Heisenberg Hamiltonian for two $S = 2$ spins: $\hat{H} = -2J_{Mn-Mn}\hat{S}_{Mn1}\cdot\hat{S}_{Mn2} + g_{Mn}\mu_B B(\hat{S}_{Mn1} + \hat{S}_{Mn2})$, where $J_{Mn-Mn}$ is the exchange interaction. Good agreement was found with $J_{Mn-Mn} = -58$ $cm^{-1}$ with fixed $g_{Mn} = 2.0$, with a small 4% monomeric impurity of $S = 2$ (Figure 2a). This conclusion is not surprising since oxide bridges are likely to lead to antiferromagnetic interactions.

The $\chi_M T(T)$ value for $\{Ni_2Y_2\}$ (**18**) at room temperature is 2.62 $cm^3$ K $mol^{-1}$ (consistent with two uncoupled $S = 1$ ions with $g = 2.29$; see Table S6, Supporting Information, and Figure 2b), decreasing only slowly down to about 100 K where it starts decreasing more rapidly. This could be due to antiferromagnetic coupling or significant single-ion anisotropy. An interesting $M_\beta(H)$ profile is observed (inset in Figure 2b), with exponential-like behavior and higher magnetization values observed at 4 than at 2 K, suggesting that paramagnetic excited states are close to an $S = 0$ ground state. Modeling the magnetic behavior of $\{Ni_2Y_2\}$ requires an additional term in the Hamiltonian because the zero-field splitting of the Ni(II) ions ($D_{Ni}$) is likely to be of the same order as the weak exchange interaction;[26] therefore, we adopt the Hamiltonian

$$\hat{H} = -2J_{Ni-Ni}\hat{S}_{Ni1}\cdot\hat{S}_{Ni2} + D_{Ni}(\hat{S}^2_{Ni2_z} - \hat{S}_{Ni1}{}^2/3 + \hat{S}^2_{Ni2_z} - \hat{S}_{Ni2}{}^2/3) + g_{Ni}\mu_B H(\hat{S}_{Ni1} + \hat{S}_{Ni2})$$

Simultaneous fitting[23] of $M_\beta(H,T)$ and $\chi_M T(T)$ provides good agreement with $J_{Ni-Ni} = -4.6$ $cm^{-1}$, $D_{Ni} = +10.3$ $cm^{-1}$, and $g_{Ni} = 2.34$.

For $\{Co_2Y_2\}$ (**6**), $\chi_M T(T)$ decreases slowly from 5.6 $cm^3$ K $mol^{-1}$ at room temperature until about 24 K, below which it quickly drops to 0.47 $cm^3$ K $mol^{-1}$ (Figure S2a, Supporting Information). Such behavior is expected from the orbitally degenerate $^4T_{1g}$ ground term of six-coordinate Co(II), with a well-isolated spin–orbit doublet ground state. $M_\beta(H,T)$ shows a cross-over feature at about 4 T (inset in Figure S2a, Supporting Information). Modeling this exchange (which is likely to be highly anisotropic) meaningfully requires further information,[27] and we do not attempt this in the present work.

*{$Mg_2Ln_2$}*. At room temperature $[Mg^{II}{}_2Gd^{III}{}_2(\mu_3\text{-}OH)_2(O_2C^tBu)_{10}][^iPr_2NH_2]_2$ (**1**) has a $\chi_M T(T)$ of 15.7 $cm^3$ K $mol^{-1}$, close to the value for two noninteracting gadolinium ions (15.6 $cm^3$ K $mol^{-1}$), and is essentially temperature independent except at very low temperatures (Figure S3a, Supporting Information). Hence, any interactions between the Gd(III) ions are very weak, consistent with the Gd···Gd distance of 6.2326(6) Å. The small downturn at low temperatures could be due to weak antiferromagnetic interactions or small zero-field splitting of the $S = 7/2$ state of each Gd(III) ion.

For all the $\{Mg_2Ln_2\}$ analogues with orbitally degenerate Ln (Tb(III), Dy(III), Ho(III), and Er(III)), room-temperature $\chi_M T(T)$ values are in good agreement with those for two uncoupled Ln(III) ions (see Table S6 and Figure S3, Supporting Information). For $\{Mg_2Dy_2\}$ (**3**), $\chi_M T(T)$ decreases slowly on cooling down to about 30 K, due to depopulation of Starks levels, below which it increases to 28.6 $cm^3$ K $mol^{-1}$ at 2 K (Figure 3). This upturn can be modeled simply by using the effective $g$ values of the ground Kramers doublet obtained from ab initio calculations (see later) and then considering the anisotropic dipole interaction between two effective spins of $S_{eff} = 1/2$. The resulting magnetic axis has an angle of 2.0° to the vector between the Dy(III) ions, and the ground doublets have effective $g$ values of $g_{xx} = g_{yy} = 0.01$ and $g_z = 19.76$ in the $S_{eff} = 1/2$ formalism. Along with the Dy···Dy distance of 6.1298(4) Å, the main component of the dipolar interaction gives $J_{zz} = +0.72$ $cm^{-1}$ (for a $-2J$ Hamiltonian). As the $g$ tensor is so axial and the two spins are coparallel, $J_{xx}$ and $J_{yy}$ are essentially zero. This value reproduces the low-temperature $\chi_M T(T)$ (where only this doublet is populated) and $M_\beta(H,T)$ well (Figure 3),[28] and it is consistent with a ferromagnetic dipolar interaction observed for reported dimeric lanthanide systems.[29]

For $\{Mg_2Tb_2\}$ (**2**), $\{Mg_2Ho_2\}$ (**4**), and $\{Mg_2Er_2\}$ (**5**), $\chi_M T(T)$ decreases only slowly to about 100 K, below which it decreases more rapidly, dominated by depopulation of the excited Stark levels (Figure S3b–d, Supporting Information). We have not tried to model any very weak exchange interactions for these complexes, since the data are insensitive to them, but the result



DOI: 10.1021/acs.inorgchem.5b00746
*Inorg. Chem.* 2015, 54, 5930–5941

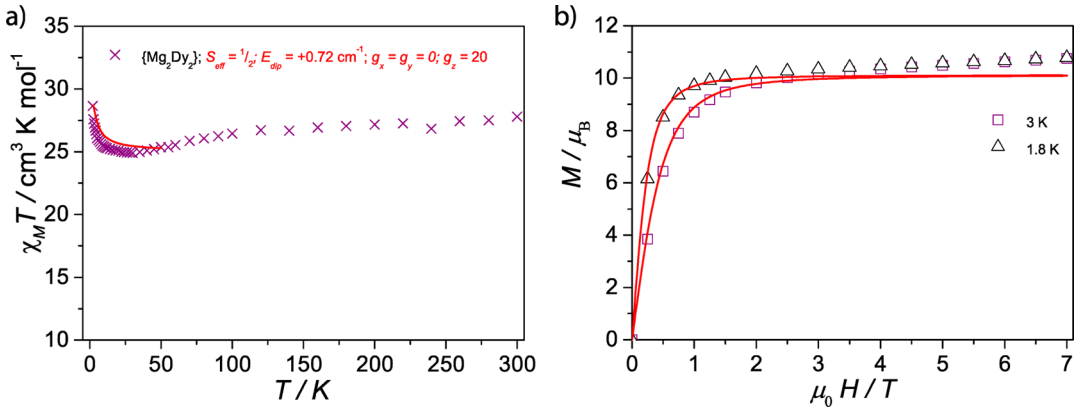


**Figure 3.** Experimental (a) $\chi_M T(T)$ and $M_\beta(H,T)$ (b) data and fits for $\{Mg_2Dy_2\}$.

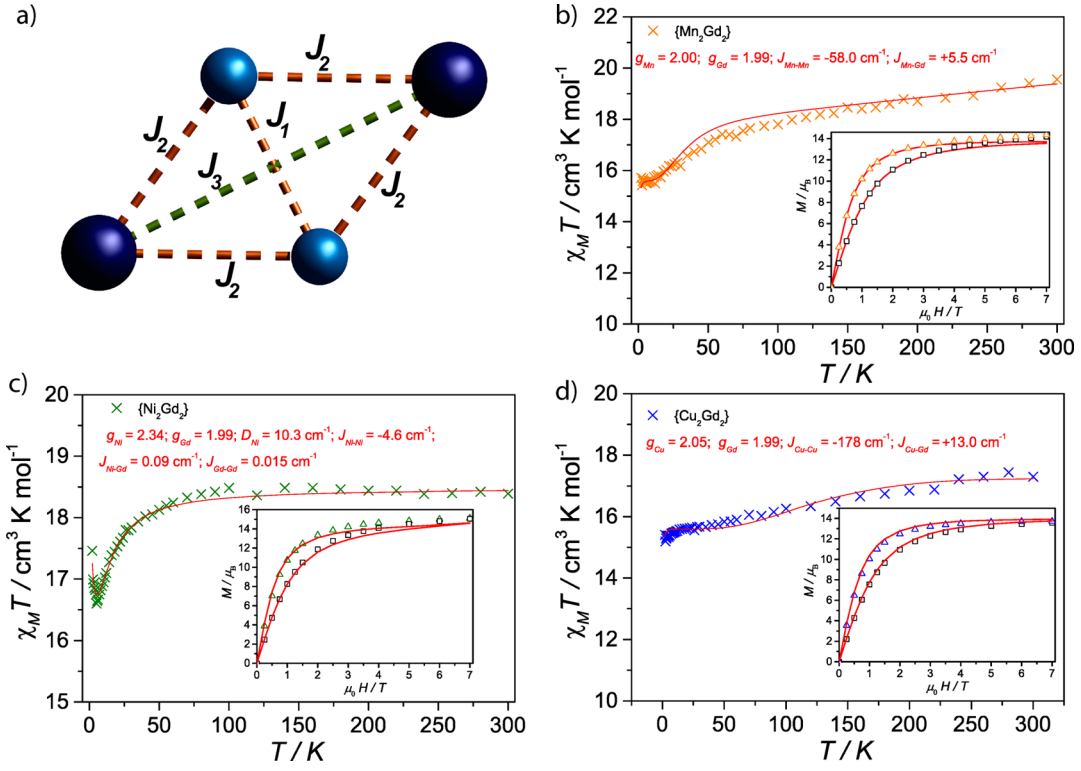


**Figure 4.** Experimental $\chi_M T(T)$ and $M_\beta(H,T)$ and simulations (red lines) for (a) $\{Ni_2Gd_2\}$ and (c) $\{Mn_2Gd_2\}$. (b) Exchange scheme.

for $\{Mg_2Dy_2\}$ suggests that the interactions are likely dipolar in nature.

*Paramagnetic Mixed-Metal Systems {$M_2Ln_2$}.* In order to gain insight into the 3d···4f interactions we first model the model $\chi_M T(T)$ and $M_\beta(H,T)$ data for the $\{M_2Gd_2\}$ complexes using the $J_{M-M}$ parameters obtained from $\{M_2Y_2\}$ where possible. The magnetic data of $\{Mn_2Gd_2\}$ has been modeled using the isotropic Hamiltonian: $\hat{H} = -2J_1(\hat{S}_{Mn1} \cdot \hat{S}_{Mn2}) - 2J_2(\hat{S}_{Mn1} + \hat{S}_{Mn2})\cdot(\hat{S}_{Gd1} + \hat{S}_{Gd2}) + \mu_B H\,(g_{Gd}(\hat{S}_{Gd1} + \hat{S}_{Gd2}) + g_{Mn}\,(\hat{S}_{Mn1} + \hat{S}_{Mn2}))$. This neglects the Gd···Gd interaction and any single-ion anisotropy. For $\{Ni_2Gd_2\}$ we allowed for the zero-field splitting of Ni(III) as in $\{Ni_2Y_2\}$ to fit the $\chi_M T(T)$ and $M_\beta(H,T)$; it was however impossible to reproduce the upturn using such approach. We therefore allow a very small Gd····Gd interaction (0.015 $cm^{-1}$) to reproduce the rise observed at low temperature using the Hamiltonian

$$\hat{H} = -2J_1(\hat{S}_{Ni1}\cdot\hat{S}_{Ni2}) - 2J_2(\hat{S}_{Ni1} + \hat{S}_{Ni2})\cdot(\hat{S}_{Gd1} + \hat{S}_{Gd2}) - 2J_3(\hat{S}_{Gd1}\cdot\hat{S}_{Gd2}) + D_{Ni}(\hat{S}^2_{Ni2_z} - \hat{S}_{Ni1}{}^2/3 + \hat{S}^2_{Ni2_z} - \hat{S}_{Ni2}{}^2/3) + \mu_B H(g_{Gd}(\hat{S}_{Gd1} + \hat{S}_{Gd2}) + g_{Ni}(\hat{S}_{Ni1} + \hat{S}_{Ni2}))$$

For $\{Mn_2Gd_2\}$ (**13**), good agreement between experiment and simulation was obtained with a ferromagnetic Mn···Gd exchange, i.e., $J_2 = +5.5$ $cm^{-1}$ where $J_1$ was fixed from $\{Mn_2Y_2\}$ (Figure 4c). Ferromagnetic Mn···Gd exchange interactions have been seen previously by several groups.[30] This was done similarly for $\{Ni_2Gd_2\}$ (**19**), with $J_1$ and $D_{Ni}$ fixed from $\{Ni_2Y_2\}$. We find good agreement for $J_2 = +0.09$ $cm^{-1}$ and $J_3 = +0.015$ $cm^{-1}$ (Figure 4a). The values of these interactions are very small, and speculation about mechanisms for the interaction seems premature.

We were unable to prepare $\{Cu_2Y_2\}$; hence, we refined $J_1$ and $J_2$ in a simultaneous fit to $\chi_M T(T)$ and $M_\beta(H,T)$ for $\{Cu_2Gd_2\}$



DOI: 10.1021/acs.inorgchem.5b00746
*Inorg. Chem.* 2015, 54, 5930−5941

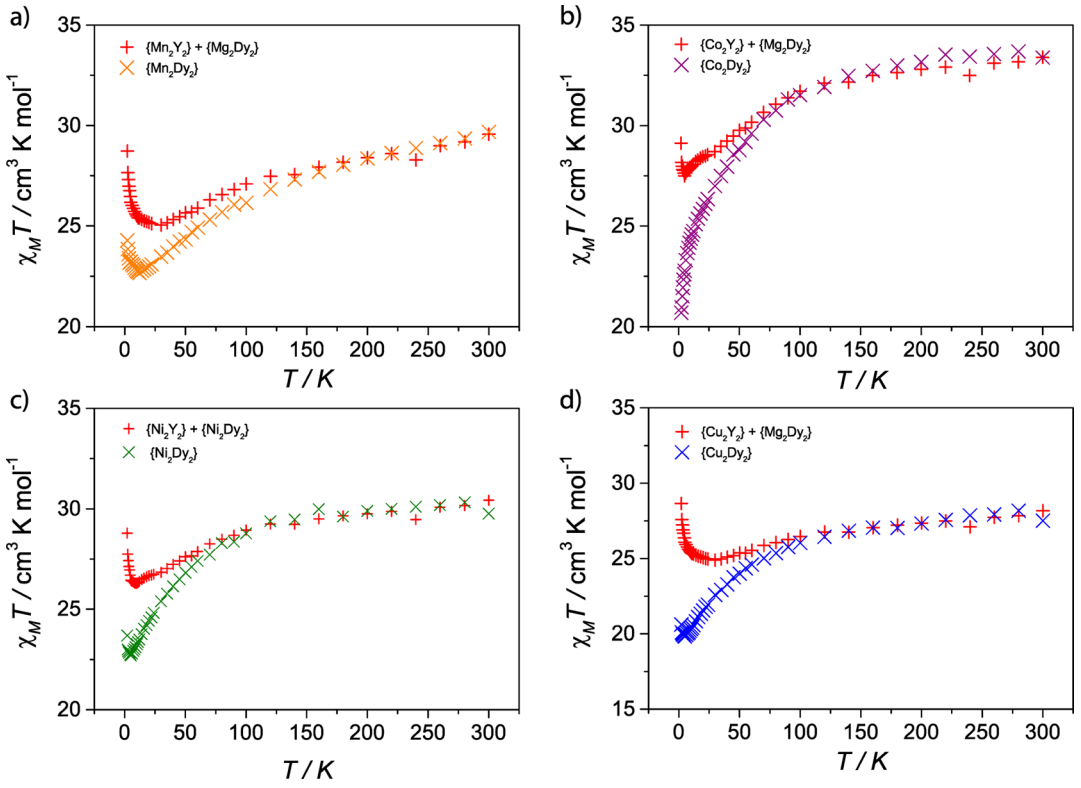


**Figure 5.** Comparison of $\chi_M T(T)$ magnetic behavior for $\{M_2Dy_2\}$ and the summed value for $\{M_2Y_2\}$ + $\{Mg_2Dy_2\}$, where M is (a) Mn, (b) Co, (c) Ni, and (d) Cu.

(**24**) giving $J_1 = -178$ cm$^{-1}$ and $J_2 = +13$ cm$^{-1}$ (Figure 4d). These values are in good agreement with related Cu···Cu[31] and Cu···Gd[11,31] pairs; however, care must be taken with the Cu···Gd value and the Mn···Gd value due to the strong Cu···Cu and Mn···Mn interaction.

While we cannot model the magnetic data for the Ln(III) = Tb, Dy, Ho, and Er analogues to obtain the 3d···4f interaction directly, some qualitative insight can be gained from comparing the sum of the data for $\{Mg_2Ln_2\}$ with $\{M_2Y_2\}$ with those from $\{M_2Ln_2\}$ (see Figures 5 and S4−S6, Supporting Information). Despite not having the $\{Cu_2Y_2\}$ analogue, some insight into the behavior of $\{Cu_2Ln_2\}$ has been achieved using the Cu···Cu exchange interaction obtained for $\{Cu_2Gd_2\}$ and simulating the $\chi_M T(T)$ for $\{Cu_2Y_2\}$.

In all cases the room-temperature $\chi_M T(T)$ values are in good agreement between the measured $\{M_2Ln_2\}$ and the composed $\{M_2Y_2\}$ + $\{Mg_2Ln_2\}$ data: this is expected as the effect of rather weak $J_{M-Ln}$ exchange interactions will be "washed out" when $kT \gg J$. Significant deviations are observed, however, at lower temperatures (Figures 5 and S4−S6, Supporting Information). For $\{M_2Dy_2\}$ the measured $\chi_M T$ values fall below the sum of the components at around 70 K for $\{Co_2Dy_2\}$, $\{Ni_2Dy_2\}$, and $\{Cu_2Dy_2\}$ and at around 150 K for $\{Mn_2Dy_2\}$, implying possible antiferromagnetic $J_{M-Dy}$ interactions. The deviation for the former three compounds continues to grow as temperature falls, while for $\{Mn_2Dy_2\}$ it remains small throughout the temperature range. It is worth noting that the low-temperature upturn is maintained in $\{Mn_2Dy_2\}$, $\{Ni_2Dy_2\}$, and $\{Cu_2Dy_2\}$ but not for $\{Co_2Dy_2\}$.

Similarly, the nature and strength of the interaction observed at low temperatures can be better observed through the $\Delta\chi_M T$ function for $\{M_2Ln_2\}$ − ($\{M_2Y_2\}$ + $\{Mg_2Ln_2\}$; ferromagnetic M···Ln behavior is expected when this function is greater than zero and antiferromagnetic if it is less than zero. For all $\{M_2Dy_2\}$ complexes the interaction is antiferromagnetic (Figure 5), which contrasts with the $\{M_2Gd_2\}$ complexes where the interaction is ferromagnetic (Figure 4). For $\{Mn_2Tb_2\}$ and $\{Ni_2Tb_2\}$ the interaction is ferromagnetic, and no firm conclusion can be drawn for $\{Co_2Tb_2\}$ and $\{Co_2Gd_2\}$ as the $\Delta\chi_M T$ function is almost invariant with temperature (Figures S6 and S7, Supporting Information). For the heavier 4f ions investigated the interactions are almost always antiferromagnetic, with the exception of $\{Ni_2Er_2\}$. These findings are summarized in Table 2.

**Table 2. 3d−4f Exchange Interaction Obtained from Simulation and Qualitative Analysis**[a]

| 3d−4f | Mn | Co | Ni | Cu |
|---|---|---|---|---|
| Gd | F | − | F | F |
| Tb | F | − | F | − |
| Dy | AF | AF | AF | AF |
| Ho | AF | AF | AF | AF |
| Er | AF | AF | F | AF |

[a]F = ferromagnetic; AF = antiferromagnetic; − = no observable difference.

Given that the approach involves some approximations, a tentative conclusion is that the exchange interaction becomes more antiferromagnetic as the number of f electrons increases, with $f^7$ ($Gd^{III}$) and $f^8$ ($Tb^{III}$) ferromagnetic and $f^9$ and greater antiferromagnetic.

*Alternating Current Magnetic Susceptibility.* Frequency- and temperature-dependent magnetic susceptibility measurements (1.55 G oscillating field) were obtained for all clusters at zero and/or 1 kG applied dc field. Frequency-dependent behavior, typical of SMMs, was observed in all $\{M_2Dy_2\}$ clusters



DOI: 10.1021/acs.inorgchem.5b00746
*Inorg. Chem.* 2015, 54, 5930−5941

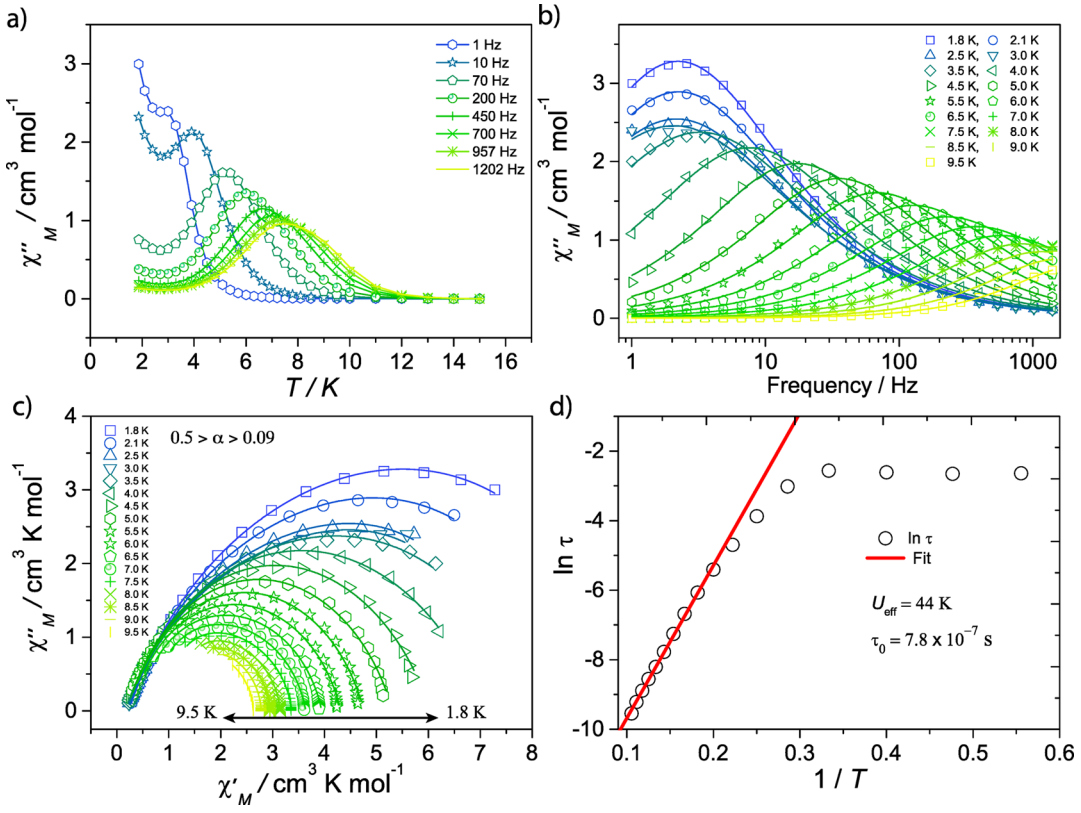


**Figure 6.** (a) $\chi''_M(T)$, (b) $\chi''_M(\nu)$, (c) Cole−Cole plot, and (d) Arrhenius analysis of $\{Mg_2Dy_2\}$ at zero dc field.

and four of the $\{M_2Er_2\}$ analogues (M = Mg(II), Mn(III), Ni(II), and Cu(II)). We first describe the behavior of the $\{M_2Y_2\}$ and $\{Mg_2Ln_2\}$ systems and then what effect the $J_{M-Ln}$ interaction has on the dynamic magnetic properties for the $\{M_2Ln_2\}$ complexes.

*{$M_2Y_2$}*. No frequency-dependent behavior was observed in nil or 1 kG applied dc field. Hence, the $\{M_2\}$ units do not give rise to SMM behavior, which is as expected due to small magnetic anisotropy and the antiferromagnetic $J_1$ interactions leading to $S = 0$ ground states.

*{$Mg_2Ln_2$}*. Clear peaks in the out-of-phase susceptibility ($\chi''_M$) as a function of temperature and frequency were observed for $\{Mg_2Dy_2\}$ (Figure 6) and $\{Mg_2Er_2\}$ (Figure 7). No out-of-phase component was observed for the Tb and Ho analogues, even with the application of a small dc field.

For $\{Mg_2Dy_2\}$ (Figure 6), $\chi''_M(T)$ has a significant out-of-phase signal below 12 K at zero dc field with a maximum at 7.5 K for the highest measurement frequency ($\nu$) of 1.2 kHz. The peaks in $\chi''_M(\nu)$ become temperature independent below 3 K, indicating a quantum regime. The tunnelling frequency was found to be 2.2 Hz, resulting in a quantum tunnelling time of ($\tau_{QTM}$) of 71 ms. At temperatures above 5 K the relaxation data is roughly linear and can be described using the Arrhenius law, $\tau = \tau_0 \exp(U_{eff}/kT)$, revealing a thermal energy barrier to magnetization relaxation of $U_{eff}$ = 44 K and $\tau_0 = 7.8 \times 10^{-7}$ s (Figure 6c and 6d). Cole−Cole plots ($\chi'_M$ vs $\chi''_M$) for the temperature range 1.8−9.5 K give temperature-dependent $\alpha$ parameters: at high temperatures $\alpha$ = 0.05, characteristic of a single relaxation time, and upon lowering the temperature $\alpha$ increases to 0.30, indicating a wider distribution of relaxation times (Figure 6c).

For $\{Mg_2Er_2\}$ (Figure 7), there is a frequency-dependent behavior of the susceptibility without applied field; this is enhanced with the application of a small dc field of 1 kG, presumably due to the suppression of quantum tunnelling of the magnetization through the anisotropy barrier. The maximum in $\chi''_M(T)$ is observed at 4 K for $\nu$ = 1.2 kHz. No temperature-independent behavior was observed in the $\chi''_M(\nu)$ susceptibility; hence, we do not reach the pure quantum regime consistent with the suppression of tunnelling. An Arrhenius fit to the high-temperature, pseudolinear region shows $U_{eff}$ = 23 K and $\tau_0 = 6.6 \times 10^{-7}$ s. Cole−Cole plots behave similarly to those for $\{Mg_2Dy_2\}$, with $\alpha$ = 0.035 at higher temperatures increasing to $\alpha$ = 0.2 at the lowest temperatures.

*Mixed Paramagnetic Metal Complexes {$M_2Ln_2$}*. $\chi''_M(T)$ for $\{Mn_2Dy_2\}$ (Figure 8) peaks around 7 K at 1.2 kHz before increasing again at lower temperatures: the peaks are broader than those observed in $\{Mg_2Dy_2\}$. $\chi''_M(\nu)$ is frequency independent below ca. 3 K. Analysis of the data gives $U_{eff}$ = 29 K with $\tau_0 = 4.6 \times 10^{-6}$ s, and the distribution of relaxation processes varies from $\alpha$ = 0.2 to 0.3 from high to low temperature. The high-temperature $\alpha$ is noticeably larger than that found for $\{Mg_2Dy_2\}$. We obtained the tunnelling frequency 27.7 Hz, which corresponds to a $\tau_{QTM}$ of 5.7 ms, larger than that obtained in $\{Mg_2Dy_2\}$.

For $\{Ni_2Dy_2\}$ the maximum in $\chi''_M(T)$ is observed at 3.5 K for 1.2 kHz (Figure 9), i.e., at a lower temperature than $\{Mg_2Dy_2\}$. Analysis of $\chi''_M(T,\nu)$ gives $U_{eff}$ = 20 K and $\tau_0 = 6.0 \times 10^{-7}$ s, with $\alpha$ varying from 0.01 to 0.1 from high to low temperature, lower than those for $\{Mg_2Dy_2\}$.

Similar behavior is observed for $\{Ni_2Er_2\}$, with a maximum in $\chi''_M(T)$ at 2.4 K under 1 kG dc field. Arrhenius analysis gives $U_{eff}$ = 18 K with $\tau_0 = 3.9 \times 10^{-6}$ s and $\alpha$ = 0.1 at high temperature, increasing to 0.2 at lower temperatures (Figure 10).

$\{M_2Dy_2\}$, where M = Co(II) and Cu(II), and $\{Cu_2Er_2\}$ exhibit out-of-phase components; however, no maxima are observed in $\chi''_M(T)$ above 2 K, making it impossible to derive an energy barrier (Figure S9, Supporting Information).



DOI: 10.1021/acs.inorgchem.5b00746
*Inorg. Chem.* 2015, 54, 5930−5941

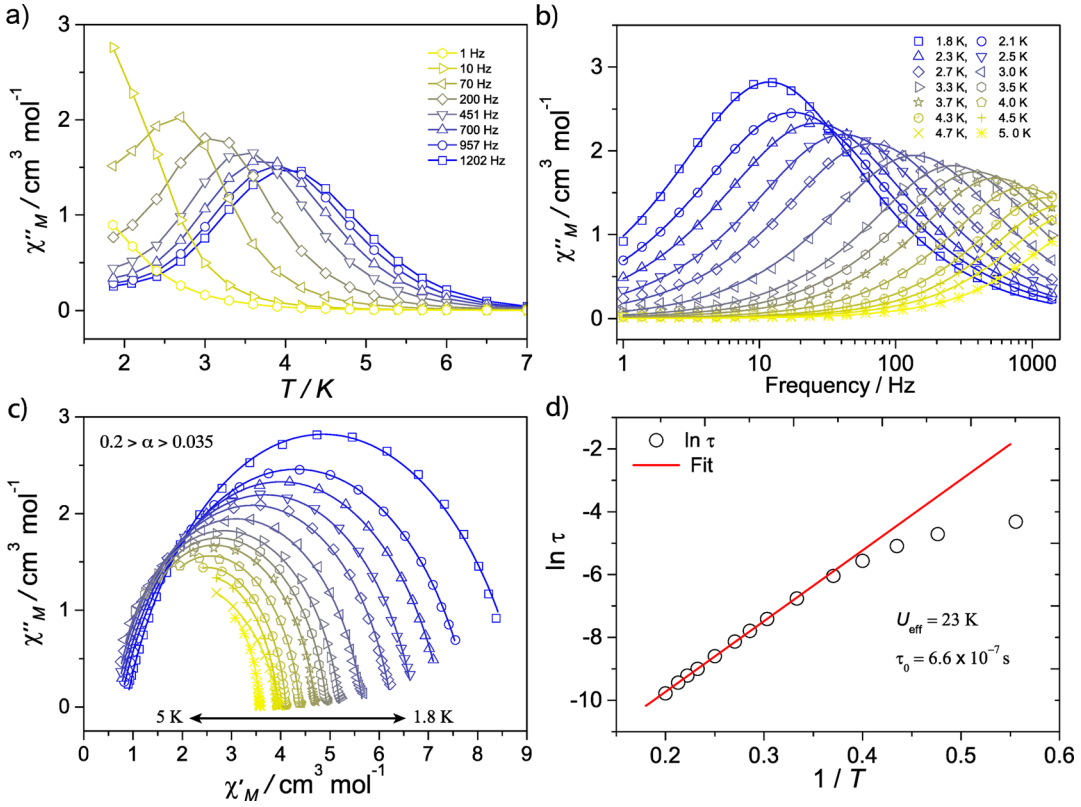


**Figure 7.** (a) $\chi''_M(T)$, (b) $\chi''_M(\nu)$, (c) Cole−Cole plot, and (d) Arrhenius analysis of $\{Mg_2Er_2\}$ measured under 1 kG dc field.

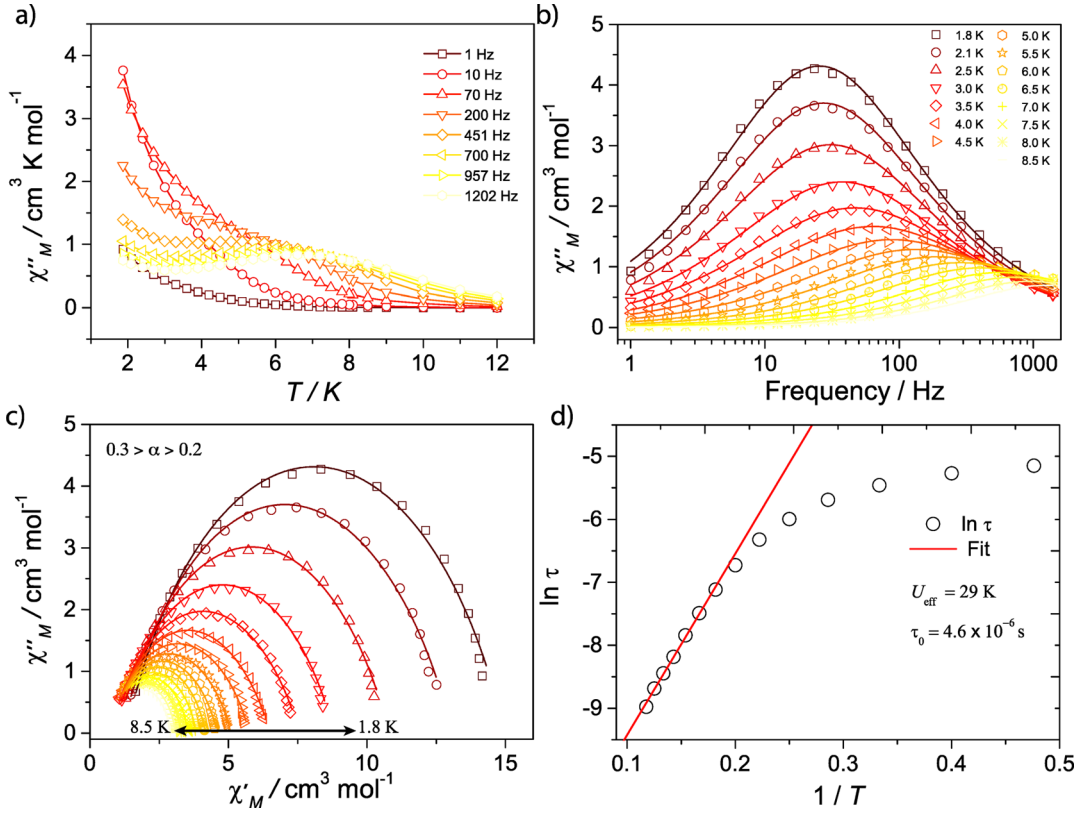


**Figure 8.** (a) $\chi''_M(T)$, (b) $\chi''_M(\nu)$, (c) Cole−Cole plot, and (d) Arrhenius analysis of $\{Mn_2Dy_2\}$ at zero dc field.

## AB INITIO CALCULATIONS

Many studies of dysprosium complexes have shown that slow relaxation of magnetization (i.e., SMM behavior) occurs when the ground state is a well-defined $m_J = \pm 15/2$ Kramers doublet. Such a state has a strongly axial effective $g$ ensor with principal values $g_{xx} = g_{yy} \approx 0$ and $g_{zz} = 20$. To understand the origin of the



DOI: 10.1021/acs.inorgchem.5b00746
*Inorg. Chem.* 2015, 54, 5930−5941

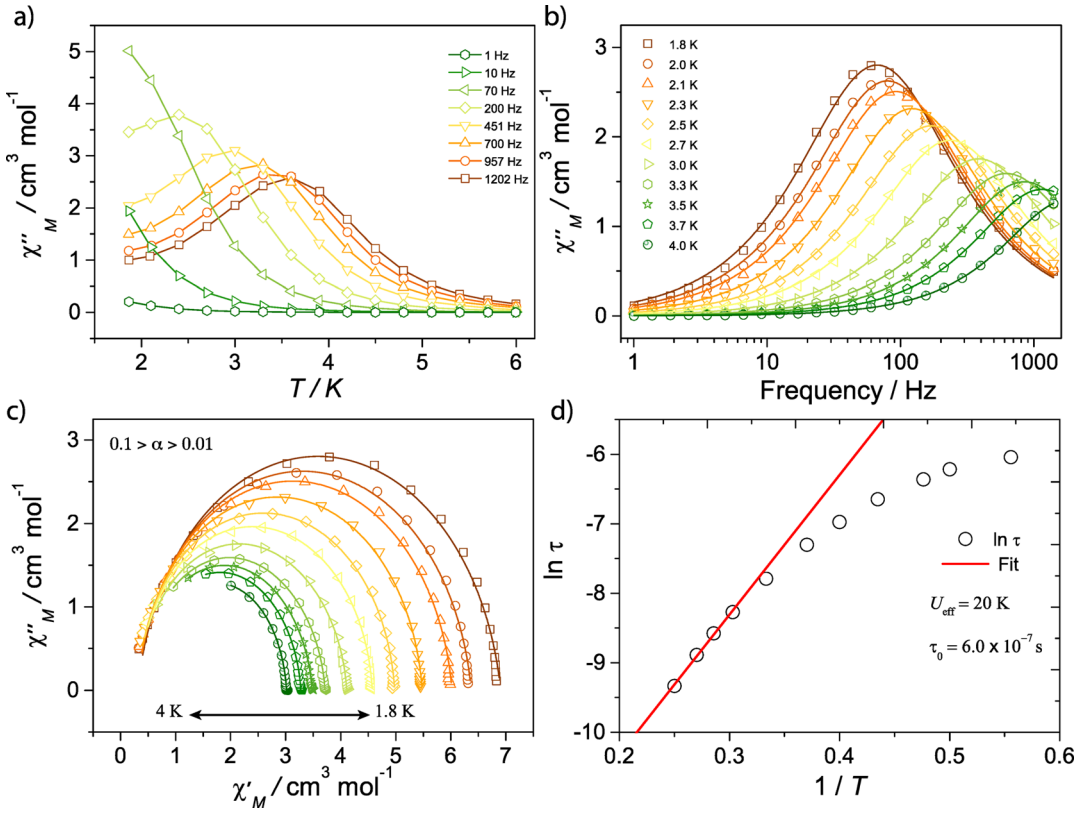


**Figure 9.** (a) $\chi''_M(T)$, (b) $\chi''_M(\nu)$, (c) Cole−Cole plot, and (d) Arrhenius analysis of $\{Ni_2Dy_2\}$ at zero dc field.

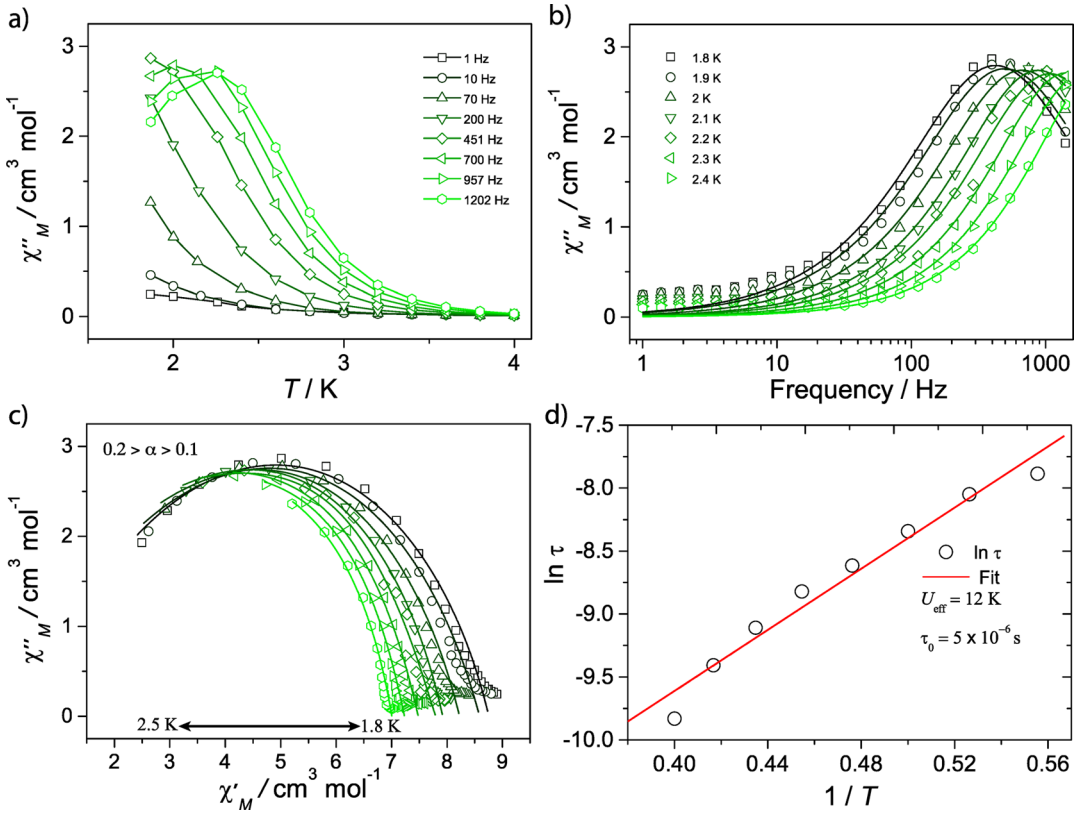


**Figure 10.** (a) Temperature-dependence $\chi''_M(T)$; (b) frequency-dependence $\chi''_M(\nu)$; (c) Cole−Cole plot; (d) energy barrier of $\{Ni_2Er_2\}$ under 1 kG applied magnetic field.



DOI: 10.1021/acs.inorgchem.5b00746
*Inorg. Chem.* 2015, 54, 5930−5941

slow magnetic relaxation in the Dy(III) clusters, we performed CASSCF (complete active space self-consistent field) ab initio calculations using MOLCAS[32−34] (see Supporting Information for details). These calculations have widely proven to be effective in the prediction and understanding of the SMM behavior. For all the present $\{M_2Dy_2\}$ clusters, the CASSCF calculations predict similar properties for the Dy(III) ions, strongly anisotropic ground doublets with $g_z$ approaching 20, while $g_x$ and $g_y$ are close to 0, with the first excited state at ∼60−140 $cm^{-1}$ (Tables S7−S11, Supporting Information). In all cases the principal magnetic axis of the ground doublet is almost coparallel with the Dy···Dy vector (see Figure 11), and the principal axis of the first excited state is not coincident with that of the ground state, with deviations of 12−29°. These results suggest that the Dy(III) ions in the $\{M_2Dy_2\}$ clusters would show some slow relaxation properties with maximum energy barriers corresponding to the first excited state. However, it is likely that the effective barriers will be much lower due to the low symmetry and lack of strong magnetic uniaxiality.

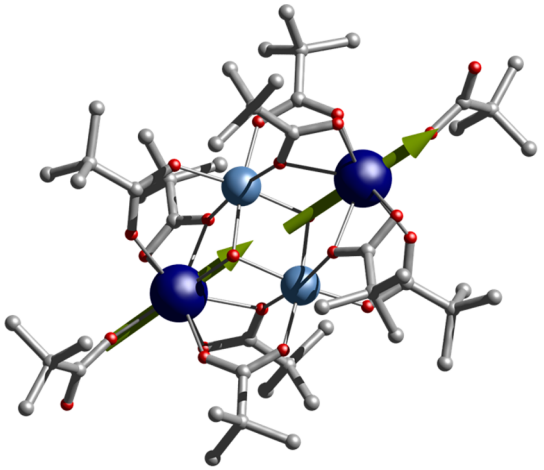

**Figure 11.** Magnetic axis calculated CASSSCF calculations for (a) $\{Mg_2Dy_2\}$ lying 2.0° off the Dy···Dy vector. Magnetic axis for the remaining $\{M_2Dy_2\}$ clusters lies close to that observed for $\{Mg_2Dy_2\}$ with small deviations, i.e., 4.0°, 3.6°, 5.4°, and 1.6° for $\{Mn_2Dy_2\}$, $\{Ni_2Dy_2\}$, $\{Cu_2Dy_2\}$, and $\{Co_2Dy_2\}$, respectively, from the Dy···Dy vector. Color code: Dy, blue; Mg, cyan; O, red; C, gray. H omitted for clarity.

## DISCUSSION

As none of the $\{M_2Y_2\}$ clusters show an out-of-phase component of the ac susceptibility, it is clear that the SMM behavior for the $\{M_2Dy_2\}$ and some of the $\{M_2Er_2\}$ compounds is due to the lanthanide ions in the molecule. The majority of 4f-SMMs reported involve Dy(III),[5] due to its propensity to have an $m_J = \pm 15/2$ doublet lowest in energy. Er-containing SMMs are less common; unfortunately Er(III) is a poor subject for ab initio calculations, and hence, calculations to explain why one Er complex is an SMM and another is not are not straightforward.

For the Dy-based systems, the maximum $\chi''_M(T)$ value at 1.2 kHz is observed for $\{Mg_2Dy_2\}$ at ∼7.5 K and shifted to lower temperatures of 6.5 and 3.5 K for $\{Mn_2Dy_2\}$ and $\{Ni_2Dy_2\}$, respectively, with no maximum above 1.8 K for $\{Co_2Dy_2\}$ or $\{Cu_2Dy_2\}$. Detailed advanced multiconfigurational ab initio has allowed us to determine the magnetic axis for all systems, leading to basically all axes being colinear with the Dy···Dy vector. A closer look at the electronic states obtained from ab initio calculation (Tables S7−S11, Supporting Information) shows all Dy(III) sites show little deviation with respect to each other, implying that in all cases small differences should be observed between systems.

The calculations suggest that the electronic differences between the individual Dy(III) sites in the various compounds are small. Therefore, any explanation of different dynamic magnetic behavior must be related to the strength of the 3d−4f exchange interactions, Table 3. To estimate the M···Dy exchange interaction in the $\{M_2Ln_2\}$ pairs where Ln is anisotropic, we consider the difference between the observed $\chi_M T_{obs}$ value at 2 K and that calculated for the sum of the appropriate $\{M_2Y_2\}$ and $\{Mg_2Ln_2\}$ compounds $\chi_M T_{sum}$ at the same temperature. In this case the individual paramagnetic ions are present, but there is no possibility of exchange. Hence, we assume $\chi_M T_{obs} - \chi_M T_{sum}$ is a reflection of the M···Dy exchange interaction. We observe that as the M···Dy interaction becomes stronger, the $U_{eff}$ barrier decreases and becomes unmeasurable for $\{Co_2Dy_2\}$ and $\{Cu_2Dy_2\}$ where the interactions seem to be the strongest. A similar conclusion seems to be evident for the $\{M_2Er_2\}$ complexes, where slow relaxation can only be quantified for $\{Mg_2Er_2\}$ (where there is no paramagnetic 3d metal present) and $\{Ni_2Er_2\}$ (where the magnetic interactions are negligible).

## CONCLUSIONS

Successful synthesis of 27 isostructural complexes has been achieved and allows us to study the magnetic behavior of the mixed 3d−4f metal systems. Dynamic magnetic susceptibility measurements show SMM behavior for all Dy-based tetramers and some Er-based molecules in zero and 1 kG dc fields, respectively. Moreover, no SMM behavior was observed for any of the molecules when just the diamagnetic yttrium analogue is present, clearly revealing that the SMM behavior observed in the Dy- and Er-based systems is intrinsic to the lanthanide ion. Ab initio calculations performed on all Dy-containing molecules reveal similar electronic structure for the Dy(III) in all systems, and therefore, it seems that the strength of the 3d−4f exchange interaction plays a key role in the SMM properties observed. Unfortunately it appears that even weak exchange interactions

**Table 3. 3d−4f Exchange Interaction Obtained from Simulation and Qualitative Analysis**

| | Ln = Gd | Ln = Dy[a] | | | | Ln = Er[b] | | | |
|---|---|---|---|---|---|---|---|---|---|
| | $J_{Gd\text{-}M}$ ($cm^{-1}$) | $(\chi_M T)_{obs} - (\chi_M T)_{sum}$[c] | $U_{eff}/k$ (K) | $\tau_o$ ($s^{-1}$) | $\alpha$[d] | $(\chi_M T)_{obs} - (\chi_M T)_{sum}$[c] | $U_{eff}/k$ (K) | $\tau_o$ ($s^{-1}$) | $\alpha$[d] |
| $\{Mg_2Ln_2\}$ | | | 44 | $7.8 \times 10^{-7}$ | 0.05 | | 23 | $6.6 \times 10^{-7}$ | 0.035 |
| $\{Mn_2Ln_2\}$ | +5.5 | −4.4 | 29 | $4.6 \times 10^{-6}$ | 0.2 | −5.3 | | | |
| $\{Co_2Ln_2\}$ | | −8.5 | | | | −1.5 | | | |
| $\{Ni_2Ln_2\}$ | +0.08 | −5.2 | 20 | $6.0 \times 10^{-7}$ | 0.01 | +0.4 | 18 | $3.9 \times 10^{-6}$ | 0.1 |
| $\{Cu_2Ln_2\}$ | | −8.0 | | | | −5.7 | | | |

[a]SMM behavior measured in zero dc field. [b]SMM behavior measured in 1 kG dc field. [c]Calculated at 2 K. [d]Value at highest measured temperature.



DOI: 10.1021/acs.inorgchem.5b00746
Inorg. Chem. 2015, 54, 5930−5941

(ferro- or antiferromagnetic) have a negative influence on the observed $U_{eff}$ value.

Similar observations have been explained previously, where the weak interaction between Ln(III) centers provides additional relaxation pathways, therefore diminishing or even quenching the dynamic magnetic behavior.[5,6c,35] However, Nojiri and co-workers used EPR experiments to study exchange interactions in M−Dy compounds and showed that strong exchange interactions are able to improve the SMM performance.[14e] Similarly, Murray and co-workers compared $Cr^{III}$−Dy and $Co^{III}$−Dy complexes and find that while similar energy barriers are observed in both species magnetic hysteresis is found in the former due to a strong $Cr^{III}$−Dy exchange interaction, which is absent in the latter.[13,17] It appears that there are three distinct regimes for M−Ln complexes: (i) where there is no exchange interaction, the dynamic magnetic behavior is due to isolated Ln ions, (ii) where there is a weak interaction present, the interaction tends to introduce further relaxation pathways for loss of magnetization and hence diminishes $U_{eff}$, and (iii) where there is a strong interaction between the paramagnetic $Ln^{III}$ site and another paramagnetic metal, which tends to disfavor QTM at zero field, leading to observation of magnetic hysteresis.[9,13]

## ■ ASSOCIATED CONTENT

### Supporting Information

Synthetic, CASSCF method and tables, elemental analysis, crystallographic and continuous-shaped measure tables, and magnetic data tables and figures for all compounds. The Supporting Information is available free of charge on the ACS Publications website at DOI: 10.1021/acs.inorgchem.5b00746.

## ■ AUTHOR INFORMATION


### Corresponding Authors

*E-mail: Richard.Winpenny@manchester.ac.uk.
*E-mail: eric.mcinnes@manchester.ac.uk;.

### Present Address

†Eufemio Moreno Pineda:

Institute of Nanotechnology, Karlsruhe Institute of Technology, D-76344, Eggenstein-Leopoldshafen, Germany.


### Notes

The authors declare no competing financial interest.

## ■ ACKNOWLEDGMENTS

E.M.P. thanks the Panamanian agency SENACYT-IFARHU for funding. R.E.P.W. thanks the Royal Society for a Wolfson Merit Award. We also thank EPSRC (UK) (grant no. EP/K039547/1) for funding for an X-ray diffractometer. N.F.C. thanks The University of Manchester for a President's Doctoral Scholarship.

## ■ REFERENCES


(1) (a) Gatteschi, D.; Sessoli, R.; Villain *J. Molecular Nanomagnets*; Oxford University Press: Oxford, U.K., 2006. (b) Winpenny, R. E. P. *Molecular Cluster Magnets*; World Scientific: London, 2012.

(2) (a) Affronte, M.; Troiani, F.; Ghirri, A.; Candini, A.; Evangelisti, M.; Corradini, V.; Carretta, S.; Santini, P.; Amoretti, G.; Tuna, F.; Timco, G.; Winpenny, R. E. P. *J. Phys. D: Appl. Phys.* **2007**, *40*, 2999−3004. (b) Mannini, M.; Pineider, F.; Sainctavit, P.; Danieli, C.; Otero, E.; Sciancalepore, C.; Talarico, A. M.; Arrio, M.-A.; Cornia, A.; Gatteschi, D.; Sessoli, R. *Nat. Mater.* **2009**, *8*, 194−197. (c) Bogani, L.; Wernsdorfer, W. *Nat. Mater.* **2008**, *7*, 179−186. (d) Leuenberger, M. N.; Loss, D. *Nature* **2001**, *410*, 789−793.

(3) (a) Roubeau, O.; Clérac, R. *Eur. J. Inorg. Chem.* **2008**, 4325−4342. (b) Glaser, T. *Chem. Commun.* **2011**, *47*, 116−130.

(4) Ishikawa, N.; Sugita, M.; Ishikawa, T.; Koshihara, S.; Kaizu, Y. *J. Am. Chem. Soc.* **2003**, *125*, 8694−8695.

(5) (a) Woodruff, D. N.; Winpenny, R. E. P.; Layfield, R. A. *Chem. Rev.* **2013**, *113*, 5110−5148. (b) Zhanga, P.; Guoa, Y.-N.; Tanga, J. *Coord. Chem. Rev.* **2013**, *257*, 1728−1763.

(6) (a) Sorace, L.; Cristiano, B. C.; Gatteschi, D. *Chem. Soc. Rev.* **2011**, *40*, 3092−3104. (b) Sessoli, R.; Powell, A. K. *Coord. Chem. Rev.* **2009**, *253*, 2328−2341. (c) Moreno-Pineda, E.; Chilton, N. F.; Marx, R.; Dörfel, M.; Sells, D. O.; Neugebauer, P.; Shang-Da, J.; Collison, D.; Slageren, S. v.; McInnes, E. J. L.; Winpenny, R. E. P. *Nat. Commun.* **2014**, *5*, 10.1038/ncomms6243.

(7) Ganivet, C. R.; Ballesteros, B.; Torre, G.; Clemente-Juan, J. M.; Coronado, E.; Torres, T. *Chem.—Eur. J.* **2013**, *19*, 1457−1465.

(8) Blagg, R. J.; Ungur, L.; Tuna, F.; Speak, J.; Comar, P.; Collison, D.; Wernsdorfer, W.; McInnes, E. J. L.; Chibotaru, L. F.; Winpenny, R. E. P. *Nat. Chem.* **2013**, *5*, 673−678.

(9) Rinehart, J. D.; Long, J. R. *Chem. Sci.* **2011**, *2*, 2078−2085. (b) Rinehart, J. D.; Fang, M.; Evans, W. J.; Long, J. R. *Nat. Chem.* **2011**, *3*, 538−542.

(10) Lodi Rizzini, C.; Krull, T.; Balashov, J. J.; Kavich, A.; Mugarza, P. S.; Miedema, P. K.; Thakur, V.; Sessi, S.; Klyatskaya, M.; Stepanow, R.; Gambardella, P. *Phys. Rev. Lett.* **2011**, *107*, 177205(1)−177205(5).

(11) (a) Bencini, A.; Benelli, C.; Caneschi, A.; Carlin, R. L.; Dei, A.; Gatteschi, D. *J. Am. Chem. Soc.* **1985**, *107*, 8128−8136. (b) Bencini, A.; Benelli, C.; Caneschi, A.; Dei, A.; Gatteschi, D. *Inorg. Chem.* **1986**, *25*, 572−575. (c) Benelli, C.; Caneschi, A.; Gatteschi, D.; Guillou, O.; Pardi, L. *Inorg. Chem.* **1990**, *29*, 1750−1755. (d) Winpenny, R. E. P. *Chem. Soc. Rev.* **1998**, *27*, 447−452 and references therein. (e) Sakamoto, M.; Manseki, K.; Okawa, H. *Coord. Chem. Rev.* **2001**, *219*, 379−414.

(12) See, for example: (a) Mishra, A.; Wernsdorfer, W.; Abboud, K. A.; Christou, G. *J. Am. Chem. Soc.* **2004**, *126*, 15648−15649. (b) Murugesu, M.; Mishra, A.; Wernsdorfer, W.; Abboud, K. A.; Christou, G. *Polyhedron* **2006**, *25*, 613−625. (c) Bhunia, A.; Gamer, M. T.; Ungur, L.; Chibotaru, L. F.; Powell, A. K.; Lan, Y.; Roesky, P. W.; Menges, F.; Riehn, C.; Niedner-Schatteburg, G. *Inorg. Chem.* **2012**, *51*, 8589−9597. (d) Zhao, L.; Wu, J.; Ke, H.; Tang, J. *Inorg. Chem.* **2014**, *53*, 3519−3525. (e) Zhao, L.; Wu, J.; Xue, S.; Tang, J. *Chem. Asia. J.* **2012**, *7*, 2419−2424. (f) Chandrasekhar, V.; Bag, P.; Speldrich, M.; Leusen, J. v.; Kögerler, P. *Inorg. Chem.* **2013**, *52*, 5035−5044. (g) Feltham, H. L. C.; Clérac, R.; Ungur, L.; Chibotaru, L. F.; Powell, A. K.; Brooker, S. *Inorg. Chem.* **2013**, *52*, 3236−3240. (h) Mishra, A.; Wernsdorfer, W.; Parsons, S.; Christou, G.; Brechin, E. K. *Chem. Commun.* **2005**, *16*, 2086−2088.

(13) (a) Langley, S. L.; Wielechowski, D. P.; Vieru, V.; Chilton, N. F.; Moubaraki, B.; Chibotaru, L. F.; Murray, K. S. *Chem. Sci.* **2014**, *5*, 3246−3256. (b) Langley, S. L.; Wielechowski, D. P.; Vieru, V.; Chilton, N. F.; Moubaraki, B.; Abrahams, B. F.; Chibotaru, L. F.; Murray, K. S. *Angew. Chem., Int. Ed.* **2013**, *52*, 12014−12019.

(14) (a) Mori, F.; Nyui, T.; Ishida, T.; Nogami, T.; Choi, K.-Y.; Nojiri, H. *J. Am. Chem. Soc.* **2006**, *128*, 1440−1441. (b) Okazawa, A.; Shimada, T.; Kojima, N.; Yoshii, S.; Nojiri, H.; Ishida, T. *Inorg. Chem.* **2013**, *52*, 13351−13355. (c) Watanabe, R.; Fujiwara, K.; Okazawa, A.; Tanaka, G.; Yoshii, S.; Hiroyuki, H.; Ishida, T. *Chem. Commun.* **2011**, *47*, 2110−2112. (d) Fujiwara, K.; Okazawa, A.; Kojima, N.; Tanaka, G.; Yoshii, S.; Nojiri, H.; Ishida, T. *Chem. Phys. Lett.* **2012**, *530*, 49−54. (e) Ishida, T.; Watanabe, R.; Fujiwara, K.; Okazawa, A.; Kojima, N.; Tanaka, G.; Yoshiic, S.; Nojiri, H. *Dalton Trans.* **2012**, *41*, 13609−13619.

(15) (a) Brechin, E. K.; Harris, S. K.; Parsons, S.; Winpenny, R. E. P. *Dalton Trans* **1997**, 1665−1666. (b) Benelli, C.; Murrie, M.; Parsons, S.; Winpenny, R. E. P. *Dalton Trans.* **1999**, 4125−4126. (c) Benelli, C.; Blake, A. J.; Milne, P. E. Y.; Rawson, J. M.; Winpenny, R. E. P. *Chem.—Eur. J.* **1995**, *1*, 614−618.

(16) (a) Mishra, A.; Wernsdorfer, W.; Parsons, S.; Christou, G.; Brechin, E. K. *Chem. Commun.* **2005**, 2086−2088. (b) Murugesu, M.; Mishra, A.; Wernsdorfer, W.; Abboud, K. A.; Christou, G. *Polyhedron* **2006**, *25*, 613−625.

(17) See, for example: (a) Langley, S. K.; Le, C.; Ungur, L.; Moubaraki, B.; Abrahams, B. F.; Chibotaru, L. F.; Murray, K. S. *Inorg. Chem.* **2015**, *54*, 3631−3642. (b) Langley, S. K.; Ungur, L.; Chilton, N. F.; Moubaraki, B.; Chibotaru, L. F.; Murray, K. S. *Inorg. Chem.* **2014**, *53*,




DOI: 10.1021/acs.inorgchem.5b00746
*Inorg. Chem.* 2015, 54, 5930−5941

4303−4315. (c) Langley, S. K.; Chilton, N. F.; Moubaraki, B.; Murray, K. S. *Chem. Commun.* **2013**, *49*, 6965−6967. (e) Langley, S. K.; Chilton, N. F.; Moubaraki, B.; Murray, K. S. *Inorg. Chem.* **2013**, *52*, 7183−7192. (f) Langley, S. K.; Chilton, N. F.; Ungur, L.; Moubaraki, B.; Chibotaru, L. F.; Murray, K. S. *Inorg. Chem.* **2012**, *51*, 11873−11881 (Dy−$Co^{III}$).

(18) See for example: (a) Peng, G.; Kostakis, G. E.; Lan, Y.; Powell, A. K. *Dalton Trans.* **2013**, *42*, 46−49. (b) Baniodeh, A.; Mereacre, V.; Magnani, N.; Lan, Y.; Wolny, J. A.; Schünemann, V.; Anson, C. E.; Powell, A. K. *Chem. Commun.* **2013**, *49*, 9666−9668. (c) Baniodeh, A.; Lan, Y.; Novitchi, G.; Mereacre, V.; Sukhanov, A.; Ferbinteanu, M.; Voronkova, V.; Anson, C. E.; Powell, A. K. *Dalton Trans.* **2013**, *42*, 8926−8938. (d) Mereacre, V.; Baniodeh, V.; Anson, C. E.; Powell, A. K. *J. Am. Chem. Soc.* **2011**, *133*, 15335−15337.

(19) (a) Mondal, K. C.; Sundt, A.; Lan, Y.; Kostakis, G. E.; Waldmann, O.; Ungur, L.; Chibotaru, L. F.; Anson, C. E.; Powell, A. K. *Angew. Chem., Int. Ed.* **2012**, *51*, 7550−7554. (b) Chesman, A. S. R.; Turner, D. R.; Berry, K. J.; Chilton, N. F.; Moubaraki, B.; Murray, K. S.; Deacon, G. B.; Batten, S. R. *Dalton Trans.* **2012**, *41*, 11402−11412. (c) Mondal, K. C.; Kostakis, G. E.; Lan, Y.; Wernsdorfer, W.; Anson, C. E.; Powell, A. K. *Inorg. Chem.* **2011**, *50*, 11604−11611. (d) Papatriantafyllopoulou, C.; Abboud, K. A.; Christou, G. *Inorg. Chem.* **2011**, *50*, 8959−8966. (e) Akhtar, M. N.; Lan, Y.; Mereacre, V.; Clérac, R.; Anson, C. E.; Powell, A. K. *Polyhedron* **2009**, *28*, 1698−1703.

(20) (a) Troyanov, S. I.; Kiseleva, E. A.; Korenev, Y. M. *Zh. Neorg. Khim.* **2005**, *50*, 629−634. (b) G. Aromí, G.; Bell, A. R.; Helliwell, M.; Raftery, J.; Teat, S. J.; Timco, G. A.; Roubeau, O.; Winpenny, R. E. P. *Chem.—Eur. J.* **2003**, *9*, 5142−5161. (c) Chaboussant, G.; Basler, R.; Güdel, H.-U.; Ochsenbein, S. T.; Parkin, A.; Parsons, S.; Rajaraman, G.; Sieber, A.; Smith, A. A.; Timco, G. A.; Winpenny, R. E. P. *Dalton Trans.* **2004**, 2758−2766. (d) Kiskin, M. A.; Fomina, I. G.; Aleksandrov, G. G.; Sidorov, A. A.; Novotortsev, V. M.; Rakitin, Y. V.; Dobrohotova, Z. V.; Ikorskii, V. N.; Shvedenkov, Y. G.; Eremenko, I. L.; Moiseev, I. I. *Inorg. Chem. Commun.* **2005**, *8*, 89−93. (e) Iljina, E.; Korjeva, A.; Kuzmina, N.; Troyanov, S.; Dunaeva, K.; Martynenko, L. *Mater. Sci. Eng.* **1993**, 234−236. (f) Fomina, I. G.; Kiskin, M. A.; Martynov, A. G.; Aleksandrov, G. G.; Dobrokhotova, Z. V.; Gorbunova, Y. G.; Shvedenkov, Y. G.; Tsivadze, A. Y.; Novotortsev, V. M.; Eremenko, I. L. *Zh. Neorg. Khim.* **2004**, *49*, 1463−1472. (g) Zoan, T. A.; Kuzmina, N. P.; Frolovskaya, S. N.; Rykov, A. N.; Mitrofanova, N. D.; Troyanov, S. I.; Pisarevsky, A. P.; Martynenko, L. I.; Korenev, Y. M. *J. Alloys Compd.* **1995**, *225*, 396−399.

(21) (a) Sheldrick, G. M. *Acta Crystallogr.* **2008**, *A64*, 112−122. (b) Dolomanov, O. V.; Bourthis, L. J.; Gildea, R. L.; Howard, J. A. K.; Puschmann, H. *J. Appl. Crystallogr.* **2009**, *42*, 339−341.

(22) Bain, G. A.; Berry, J. F. *J. Chem. Educ.* **2008**, *85*, 532−536.

(23) Chilton, N. F.; Anderson, R. P.; Turner, L. D.; Soncini, A.; Murray, K. S. *J. Comput. Chem.* **2013**, *34*, 1164−1175.

(24) (a) Burkovskaya, N. P.; Orlova, E. V.; Kiskin, M. A.; Efimov, N. N.; Bogomyakov, A. S.; Fedin, M. V.; Kolotilov, S. V.; Minin, V. V.; Aleksandrov, G. G.; Sidorov, A. A.; Ovcharenko, V. I.; Novotortsev, V. M.; Eremenko, I. L.; Nauk, I. A. *Russ. Chem. Bull.* **2011**, 2442. (b) Nefedov, S. E.; Kozitsyna, N. Yu.; Vargaftik, M. N.; Moiseev, I. I. *Polyhedron* **2009**, *28*, 172. (c) Mukherjee, S.; Daniels, M. R.; Bagai, R.; Abboud, K. A.; Christou, G.; Lampropoulos, C. *Polyhedron* **2010**, *29*, 54−65.

(25) (a) D. Casanova, D.; Alemany, P.; Bofill, J. M.; Alvarez, S. *Chem.—Eur. J.* **2003**, *9*, 1281−1285. (b) Alvarez, S.; Alemany, P.; Casanova, D.; Cirera, J.; Llunell, M.; Avnir, D. *Coord. Chem. Rev.* **2005**, *249*, 1693−1708.

(26) Walsh, J.; Sproules, S.; Chilton, N. F.; Barra, A.-L.; Timco, G. A.; Collison, D.; McInnes, E. J. L.; Winpenny, R. E. P. *Inorg. Chem.* **2014**, *53*, 8464−8472.

(27) Boeer, A. B.; Barra, A.-L.; Chibotaru, L. F.; Collison, D.; McInnes, E. J. L.; Mole, R. A.; Simeoni, G. G.; Timco, G. A.; Ungur, L.; Unruh, T.; Winpenny, R. E. P. *Angew. Chem., Int. Ed.* **2011**, *50*, 4007−4011. (b) Lines, M. E. *J. Chem. Phys.* **1971**, *55*, 2977−2984. (c) Lloret, F.; Julve, M.; Cano, J.; Ruiz-García, R.; Pardo, E. *Inorg. Chim. Acta* **2008**, *361*, 3432−3445.

(28) Abragam, A.; Bleaney, B. *Electron Paramagnetic Resonance of Transition Metal Ions*; Oxford University Press: Oxford, U.K., 2012.

(29) Leng, J.-D.; Liu, J.-L.; Lin, W.-Q.; Gomez-Coca, S.; Aravena, D.; Ruiz, E.; Tong, M.-L. *Chem. Commun.* **2013**, *49*, 9341−9343.

(30) See, for example: (a) Prasad, T. K.; Rajasekharan, M. V.; Costes, J.-P. *Angew. Chem., Int. Ed.* **2007**, *46*, 2851−2854. (b) Benelli, C.; Murrie, M.; Parsons, S.; Winpenny, R. E. P. *J. Chem. Soc., Dalton Trans.* **1999**, 4125. (c) Yamaguchi, T.; Costes, J.-P.; Kishima, Y.; Kojima, M.; Sunatsuki, Y.; Bréfuel, N.; Tuchagues, J.-P.; Vendier, L.; Wernsdorfer, W. *Inorg. Chem.* **2010**, *49*, 9125−9135. (d) Costes, J.-P.; Garcia-Tojal, J.; Tuchagues, J.-P.; Vendier, L. *Eur. J. Inorg. Chem.* **2009**, 3801−3806.

(31) Kahn, O. *Molecular Magnetism*; VCH: New York, 1993.

(32) Aquilante, F.; De Vico, L.; Ferre, N.; Ghigo, G.; Malmqvist, P.-A.; Neogrady, P.; Pedersen, T. B.; Pitonak, M.; Reiher, M.; Roos, B. O.; Serrano-Andres, L.; Urban, M.; Veryazov, V.; Lindh, R. *J. Comput. Chem.* **2010**, *31*, 224−247.

(33) Karlstrom, G.; Lindh, R.; Malmqvist, P. A.; Roos, B. O.; Ryde, U.; Veryazov, V.; Widmark, P. O.; Cossi, M.; Schimmelpfennig, B.; Neogrady, P.; Seijo, L. *Comput. Mater. Sci.* **2003**, *28*, 222−239.

(34) Veryazov, V.; Widmark, P. O.; Serrano-Andres, L.; Lindh, R.; Roos, B. O. *Int. J. Quantum Chem.* **2004**, *100*, 626−635.

(35) Bhunia, A.; Gamer, M. T.; Ungur, L.; Chibotaru, L. F.; Powell, A. K.; Lan, Y.; Roesky, P. W.; Menges, F.; Riehn, C.; Niedner-Schatteburg, G. *Inorg. Chem.* **2012**, *51*, 9589−9597.

(36) Rinck, J.; Novitchi, G.; Heuvel, W. V. d.; Ungur, L.; Lan, Y.; Wernsdorfer, W.; Anson, C. E.; Chibotaru, L. F.; Powell, A. K. *Angew. Chem., Int. Ed.* **2010**, *49*, 7583−7587.



DOI: 10.1021/acs.inorgchem.5b00746
*Inorg. Chem.* 2015, 54, 5930−5941